

Spectral Analysis of Lead Tailings in Topsoil

**Odumosu Joseph O^{1,2}, Nwadiolor Jonathan I¹, Alamba, Dauda¹
& Adetunji Oluwatobi O¹**

¹Department of Surveying & Geoinformatics, Federal University of Technology, Minna

²Department of Surveying & Geoinformatics, Federal University Oye Ekiti, Ekiti

Corresponding Author: odumossu4life@yahoo.com

Abstract

The adverse effect of high concentration of heavy metals, especially lead (Pb), in topsoil which include food scarcity, increase morbidity rate (due to lead poisoning) especially in children in the rural areas is alarming and requires an urgent attention. Efforts has been made by many researchers to detect lead metals in soil especially in regions where anthropogenic activities aggravates the natural occurrence of lead (Pb). Laboratory approach which involves biological and chemical analysis is limited; quite expensive, time taking and cannot measure extent of spread of this metal in a large area. Advances in geospatial science has brought a huge change in environmental studies. Herein, spectral analysis of lead tailings in topsoil was carried out, using Minna metropolis as a case study. Three different geospatial approaches of processing satellite imageries were employed – a modified Kaufmann's relation, self-developed Normalized Differential Lead Index (NDLI) and Principal Component Analysis to identify the extent of lead pollution within this study area. Results from these three techniques characterized lead tailings in the study area and comparison of the performance of all three techniques reveal that there is high level of consistency in their outputs, thus, the mapped lead spread in the study area is quite reliable. Seven (7) lead hotspots with NDLI values ranging from 13-15 were detected in the central region of the study area where built-up area is thickest, implying that human activities truly induce concentration of lead metal in topsoil. Atomic Absorption Spectrometry test carried out on soil samples taken from the identified hotspots confirm that the lead concentration in the identified areas is higher than that of other areas. The AAS results further confirmed the reliability of the developed NDLI which gives higher lead index for areas with high lead concentrates and vice versa.

Keywords: Band rationing, Kaufmann relation, Lead, NDLI, Principal Component Analysis

Introduction

Lead (Pb) is a highly toxic and heavy metal; yet it is regarded as the most important element in the environment (Latif *et al.*, 2013). It is dense (about 5gcm⁻³), soft, malleable and easily extractible. Consequently, it has become the best choice of most manufacturers. Due to these attributes, it has been commonly used for centuries (Jackson, 2021). Lead metal occurs naturally in the biosphere, however, anthropogenic and industrial activities such as mining, burning of fossil fuels, smelting, among others increase their concentration in

the environment, hence, induce their toxicity.

When the concentration of this heavy metals becomes more than the prescribed level, life-threatening problems including cancer, atherosclerosis, Alzheimer disease, and Parkinson disorder, may result, hence, posing a lot of danger to human health (Muszynska and Hanus-Fajerska, 2015). For this reason, rules and regulations in highly developed countries like the United States now prohibit the use of lead in common products such as gasoline and paint, yet lead poisoning still remains a

threat to human health especially in most Africa Countries (Kolawole *et al.*, 2018; Ilugbo *et al.*, 2018; Seema *et al.*, 2013; Latif *et al.*, 2013).

According to World Health Organization (2021), Young children are particularly vulnerable to the toxic effects of lead and can suffer profound and permanent adverse health impacts, particularly on the development of the brain and nervous system. Children get lead into their bodies by putting the lead-containing objects in their mouths, this is worst among children of the illiterates who are allowed to play with contaminated soil (Jacquelyn 2018). One of the most common sources of Lead contamination in children is from top soils.

The conventional approaches (physical, chemical and biological processes) of detecting and remediating lead metal in soil are quite cumbersome, time taking and expensive. Aside this ineffectiveness, these approaches which involve series of laboratory examination of soil is not capable of marking the extent of lead poisoning in soil of a geographical location. Physical technique is one of the approaches that have been employed by various studies for the analysis of lead in soil. This approach involves various analytical techniques, such as X-ray diffraction, toxicity characteristic leaching procedure (TCLP), the European Community Bureau of Reference (BCR), and scanning electron microscopy-energy dispersive spectrometry for the detection of lead in soil (Yin and Shi, 2014; Dhirendra and Ekhlague, 2021). These authors all recommended a swifter and robust approach of detecting lead in soil. This is the same for studies where chemical and biological approaches were employed (Yang *et al.*, 2018; Sruthi and Jayalekshmi 2014; Grobelak and Napora 2015; Azubuike *et al.*, 2016; Souza *et al.*, 2013; Xie *et al.*, 2018; Dhirendra and Ekhlague 2021).

In order to address the overwhelming problem of detecting lead metal contamination of soil, this study presents a fast, easy and near-real-time monitoring approach which involves the spectral

analysis of soils using remote sensing. The study conforms with the works of Zhao *et al.*, (2019), who used spectral analysis of soil via RS to proffer solutions to environmental problems.

Spectral reflectance of lead metal in soil

Soils contaminated by lead metals show spectral characteristics that differ from uncontaminated soils (Jin *et al.*, 2018). The spectral reflectance of Pb contaminated soils shows an increasing trend between 500 and 780nm (equivalent to the spectral range of bands 2 to 4 of landsat 8 imagery) and a decreasing trend between 780 and 900nm (band 5 of landsat 8). The reflectance of satellite images showing polluted soils exhibits increasing trend in the range 1200-2500nm (equivalent to the short wavelength infrared bands of Landsat 8 imagery – bands 6 and 7) (Yun *et al.*, 2021).

Previous studies have utilized these geospatial understanding for advancing the mapping of heavy (lead) metals in soil. Qu *et al.* (2015) exploited hyperspectral imagery involving multispectral characteristics to estimate the concentrations of lead in soil using regression analysis. Yang *et al.* (2016) assessed the performance of multiple vegetation indices derived from hyperspectral imagery to estimate the concentration of lead in soils. Wang and Gao (2018) summarized some studies carried out on the estimation of heavy (lead) metal concentrations in soil based on different data sources and highlighted the challenges and unresolved issues.

Peng *et al.* (2016) proposed the use of Landsat 8 imagery to extract spectral indices, in combination with auxiliary data like proximity of area of interest to road, which were then utilized to establish a model for estimating the heavy (lead) metals concentration in soils. Also, Liu *et al.* (2018) used Sentinel -2A imagery to investigate the areas exerted by lead metal in soils on crops. Yun *et al.* (2021) in order to improve the accuracy of mapping heavy (lead) metals in soil, integrated Landsat 8

imagery with a digital elevation model and geochemical data obtained from soil samples. The study was carried out over China and the findings of the research was consistent with the ground survey results for the study area.

Based on the understanding of spectral reflectance of lead metals in topsoil, this study aimed at detecting and mapping lead metal tailings in topsoil. Like the previous studies lead detection in this study is based on the principle of band ratioing; but the difference in approach here is that two different band ratios are combined in order to identify the lead contaminated areas. The band ratios used were (i) a self-developed lead index) and (ii) the Kaufmann's relation using the Landsat 8 OLI images. Thereafter, Principal component analysis (PCA) of the of the Landsat image was further analyzed to further demonstrate the presence of lead contamination within the study area. This study was exemplified using Minna metropolis of Niger State, Nigeria where

anthropogenic activities are expected to have increase the concentration of lead (Pb) in topsoil.

Study Area

This study was exemplified over Minna metropolis. Minna Metropolis is the most populated part of the capital city of Niger State in Nigeria. This geographical location (as seen in figure 1) lies between Latitude $09^{\circ}25' 00''$ North - $09^{\circ} 40' 00''$ North and Longitude $6^{\circ} 24' 20''$ East - $6^{\circ} 36' 40''$ East. It occupies an area of about 12200 hectares of land (Minna Master Plan, 1979). As presented in Figure 1, it is bounded in the North by Shiroro Local Government, in the East by Muan Local Government, to the West by Bosso Local Government and to the South by Paikoro Local Government areas. The population of the city is estimated at 304,113 (National Population Census 2006) and there are a lot of industrial activities carried out within the area.

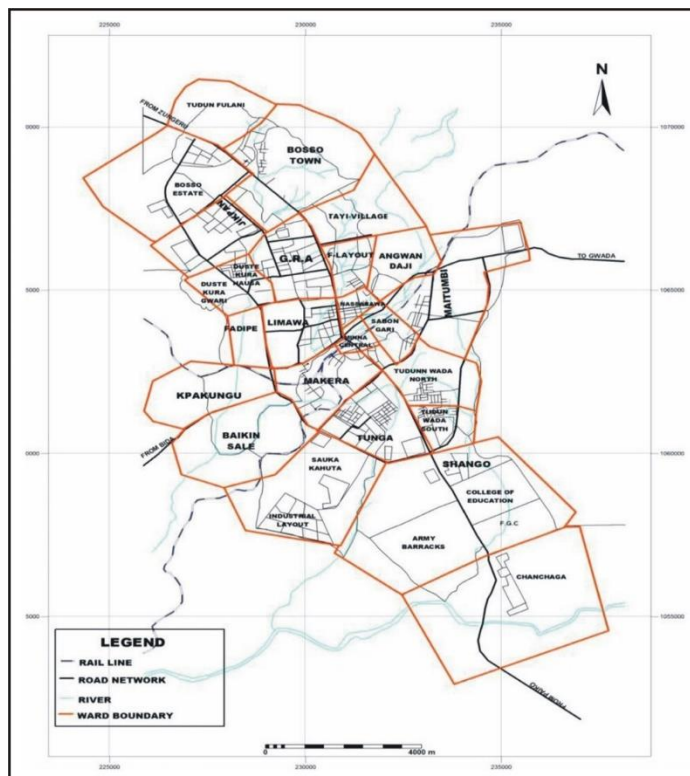


Figure 1: Study area

Methods and Materials

Materials

Table 1 and 2 respectively show the list of equipment and software used in this scientific work and the purpose which each of them served.

Methods

Figure 2 shows the schematic diagram of the methods employed in the study. The various techniques employed for data acquisition, processing and analysis of research results are discussed here under.

Satellite images were obtained from secondary sources. Landsat 8 OLI satellite imagery (path 188, row 054) covering the study area with its 9 spectral bands were downloaded. The satellite image had a horizontal resolution of 30m and was acquired from USGS Earth explorer website (www.earthexplorer.usgs.gov). Soil samples that were used for validation of the results were taken from selected locations across the study area by collecting samples into well labelled cylindrical flasks.

As seen in Figure 2, the Landsat image was first classified in order to determine the major land uses within the study area. The essence of the classification is to identify a-priori, areas where human activities are likely to increase the natural lead concentration of the soil within such areas. For this study, the maximum likelihood classifier was used alongside the ERDAS imagine 14.0 software to classify the study area.

As earlier mentioned, two band combinations were utilized in this study. The first was the Kaufmann's relation then development of a Normalized Differential Lead Index (NDLI). Earlier studies have shown that the Kaufmann's relation is optimum for determination of hydro-thermal alteration zones (Aransiola and Odumosu, 2021). It is achieved in Landsat TM by combining bands 7, 4, 3 and 5 (Ibrahim *et al.*, 2021). One band is ratioed over the other and this is done for three combinations, outputs composited as red, green and blue bands (RGB). Usually, the band ratios used for the Kaufmann ratio correspond to clay minerals, silification and ferrous mineral formations. These four bands (7,4,3 and 5) of Landsat TM are respectively equivalent to band 7, 5, 4 and 6 in Landsat 8. This band ratios and compositing have been found effective in detecting and mapping minerals, hydro-thermally altered rocks, meta-sediments and geological determination (Sadiya and Ozigis, 2015; Ibrahim *et al.*, 2021; Krishnendu *et al.*, 2019). The Kaufmann's relation is expressed as (7/5, 5/4 and 6/7) in the RGB combination (Mila and Fujimitsu, 2012). The choice of the Kaufmann's relation for detection of likely lead contamination is premised upon the fact that Lead could occur as geological meta-sediments or sediments from unregulated rudimentary processing of illegally mined lead-rich gold ore, automobile engines or other anthropogenic causes (Nabulo *et al.*, 2012). The spectral ratioing was achieved ArcMap software.

Table 1: Equipment used

Equipment	Purpose
DELL Personal Computer	For the processing of satellite imageries, processing and analysis of the same
Handheld GPS Receiver Etrex	For locating positions of soil samples mapped to be hotspot of contaminated soil
Cylindrical flask, spatula, among others	Used in the AAS laboratory test for soil test

Table 2: Software used

Software	Purpose
ArcGIS 10.4	Implementation of NDLI, Kaufmann's relation and PCA
ERDAS Imagine 14.0	For image classification
Microsoft office	Report writing and numeric data entry

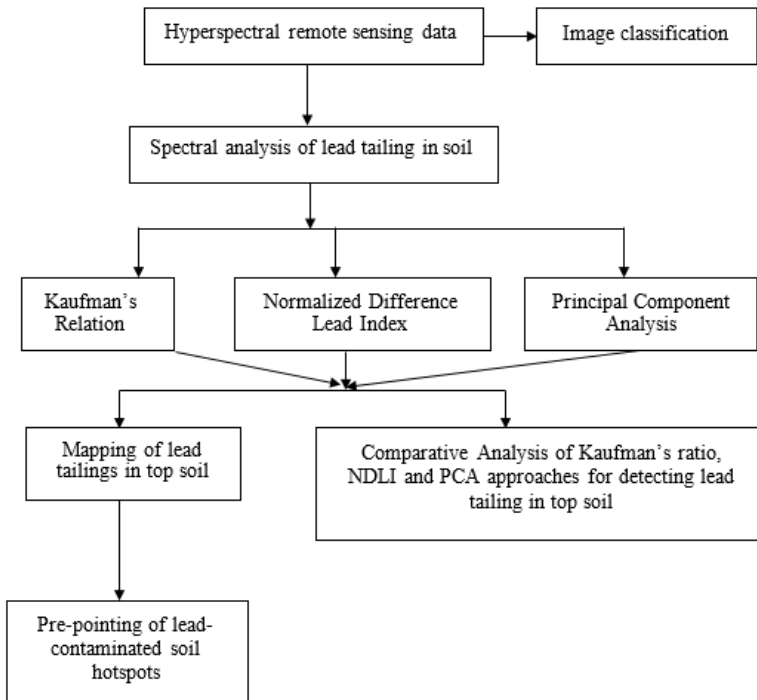


Figure 2: Methodology

The self-developed Normalized Differential Lead Index (NDLI) was achieved using specified colour combinations. Since earlier studies have shown that Lead has high spectral reflectance in the visible (500 and 780nm) and shortwave infrared (1200 – 2500nm), a band ratio of green, red and shortwave infrared as shown in equation (1) was used for the NDLI.

$$NDLI = \frac{10 \times (Band\ 3 + Band\ 4 + Band\ 6)}{(Band\ 5 + Band\ 6)} \quad (1)$$

This was implemented using the ‘Raster calculator’ of ArcMap. Raster calculator is a spatial analyst tool in ArcMap which allows raster images (or bands) to be mathematically combined. The tool creates and implements a map algebra expression that will give a raster output. In doing this, just like in programming, syntax rules of combining the raster datasets using the addition, multiplication and division operators in the order of equation 1.

The principal component analysis (PCA) method is based on the fact that neighboring bands of multispectral images are highly

correlated and often convey almost the same information about the object. This method is based on multivariate statistical technique that selects uncorrelated linear combination (eigenvector) of variables in such a way that each successively extracted linear combination – principal component. Equation (2) is an expression of the mathematical formulation that implements PCA.

$$S = \sum_i \sum_j (z_{ij} - x_i p_j)^2 \quad (2)$$

Where: z_{ij} = original data, index i stands for the variable number and j for the observation number.

p_j = the principal component which is used with a set of coefficients x_i to approximate the j th observation of the i th variable z_{ij} as $x_i p_j$. The values of the x_i 's and the p_j are to be chosen so as to minimize the sum of the squared deviations between the actual data.

The principal component analysis (PCA) is employed in the study in order to reduce the dimensionality of the datasets and validate the results from the two band rationing approaches earlier mentioned. The four bands of the Landsat 8 OLI covering the

area of interest were analyzed for the purpose of deducting the principal components, and hence, for detecting presence of lead metals across the study area.

Upon completion of the three independent processes, outputs of each were mapped over the area of interest. In order to check for the reliability and correlation between the techniques, the lead tailings mapped by each of them were assessed on the output raster bands. Principles of image interpretation were employed to detect similarities or differences in the output raster of the three techniques under study. Pattern and shape (two out of the seven elements of image interpretation in remote sensing) formed the major basis of comparison between outputs of the two approaches. The spatial distribution of lead tailings on each of the raster outputs (Kauffman, NDLI and PCA) was vectorized using polygon tool in ArcMap; this involved tracing of boundary of lead tailings. The polygons formed from the vectorized boundary of lead tailings were compared and a total conformity was noticed.

After identifying the level / extent of Lead contamination in the top soil within the study area using remote sensing, specific areas identified (based on the NDLI map as Lead hotspots were physically visited for ground truthing. Lead hotspot areas are

places where the raster cells have NDLI values ranging from 13 – 15. Seven of such spots were identified on the map and their coordinates extracted using ArcMap. Soil samples were thereafter taken from these seven hotspots and taken to the laboratory for Atomic Absorption Spectrometric (AAS) test.

Results

For the purpose of discriminating and identifying the various land cover classes within the study area, image classification was performed as earlier discussed and the result shown in Table 3 and figure 3. The built-up areas are mostly surrounded by soil covers, while the study area is largely covered by vegetation. Though lead (Pb) metal naturally occurs in the environment, its existence becomes hazardous when its concentration is attenuated by industrial activities around built-up areas. Therefore, it is expected that the spread of lead within the study area will be more around the built-up area.

Table 3 shows the distribution of the different land cover classes and land uses within the study area. Raster count of each of the classes was used to compute the extent of area (in hectares) covered by each of them. The table indicates that the soil covers 22.8% of the total area equivalent to 2780.3 hectares, next to vegetation cover.

Table 3: Analysis on land use land cover classes of the study area

S/No	Land cover/land use	Raster count	Area (hectares)	% Coverage
1.	Built up areas	12616	1135.447	9.3
2.	Soil	30892	2780.298	22.8
3.	Vegetation	87331	7859.840	64.3
4.	Water bodies	4885	439.653	3.6
	Total	135724	12215.237	100

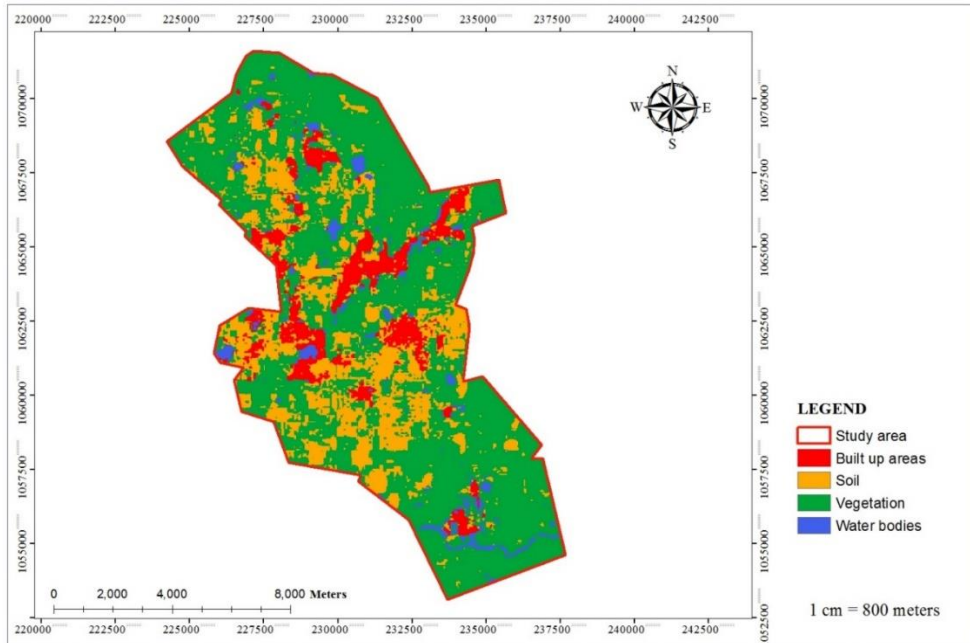


Figure 3: Land use land cover map of Minna metropolis

The Kaufmann's relation involves compositing ratioed bands. Direct implementation of the Kaufmann's relation as propounded by Kauffman, showed no traces of lead tailings within the study area. This can be attributed to the fact that the study area does not show any sign of hydro-thermal alteration hence no underground minerals within the study area. However, tweaking this relation for each of the pairs of bands and changing the combination to 7+5, 5+4, 7+6, tailings of lead were observed as seen in Figures 4(a – c) and 5. Addition of bands 7 + 5, 5 + 4 and 7 + 6 yields spectral wavelengths within the SWIR band and slightly beyond it i.e. $1.52\mu\text{m} - 3.89\mu\text{m}$.

Figure 4(a) shows additive bands 7 + 5 that is, instead of dividing the digital number (DN) of bands 7 by that of band 5, they were rather added to enhance the detection of lead. Regions with low DN values are the very dark spots and those with high values are the bright regions. The dark spots are distributed around built-up areas, where anthropogenic activities probably must have attenuated the presence of lead in top soil. The map therefore shows that the intensity

of lead in top soil inversely proportionate with the DN values in the additive combination of bands 7 and 5. Shining raster cells as observed in figure 4 has locations corresponding to vegetative areas (when compared with figure 4), and are mostly noticeable in the northern region of the study area, implying that this mathematical combination of the two bands can be explored for detection of other earth conditions within the study area. This however is left to further studies that is not covered within the scope of this study.

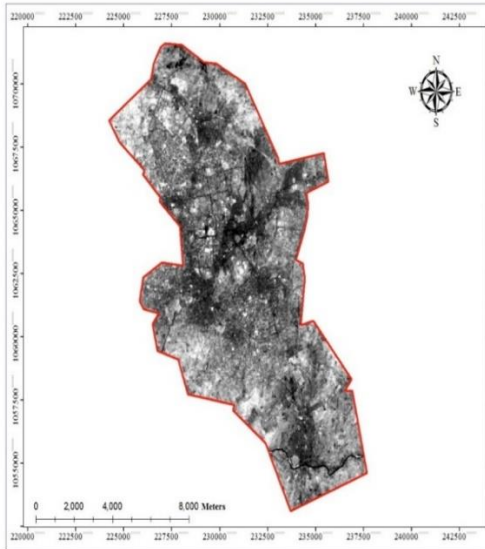


Figure 4(a): Landsat 8 bands (7+5) image

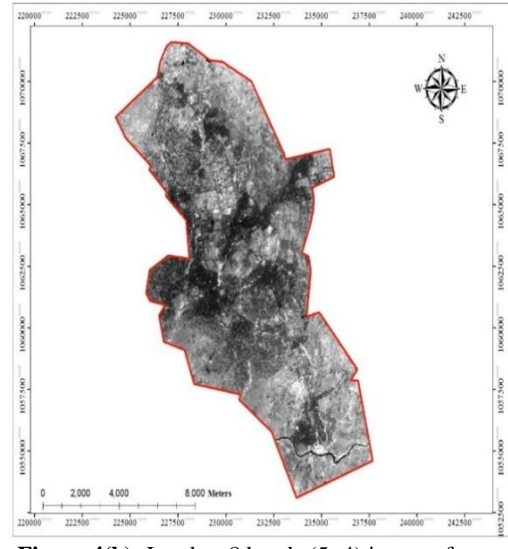


Figure 4(b): Landsat 8 bands (5+4) image of the study area

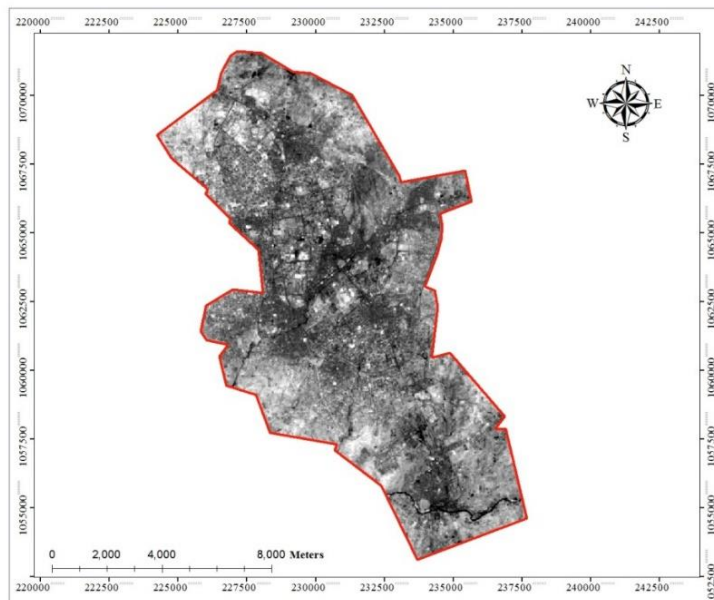


Figure 4(c): Landsat 8 bands (7+5) image

Figure 4(b) is the output of band 5 and band 4 combinations. As a modification to Kaufmann's relation (fitly applicable for detecting minerals), bands 5 and 4 were additively combined to investigate the presence of lead tailings in soil. The same pattern of distribution of low DN values observable as dark raster cells seen in figure 4(a) is also seen in figure 4(b). This implies that these two relations involving additive

combinations of spectral bands enhance the presence of lead metal in the soil. However, contrary to figure 4(a), the shining regions of figure 4(b) (reflecting very high DN values from the bands combination) are few and are noticed in the southern region of the study area.

Figure 4(c) is also an additive bands combination of bands 7 and 6. Output of

these relationship has almost the same pattern with that of figure 4 (combinations of bands 7 and 5); regions with low DN values (with locations clustering around the built-up areas) in figure 4(c) are the same in figure 4(a). Also, regions with high DN values indicated by bright tones in the study area as seen in figure 4(c) are also synonymous with that of figure 4(a). As earlier identified, the similarity in these results is traceable to the electromagnetic characters of band 5, 6 and 7 of Landsat 8 OLI. Channels 6 and 7 are within the short wavelength infrared with wavelength ranges 1.56-1.66 μ m and 2.10-2.30 μ m respectively. Suggestively, these bands can be used interchangeably to map any Earth objects that transmits signal in SWIR.

Figure 5 shows a colour composite of figures 4(a) – (c). The map indicated the probable top soil regions polluted with high concentration of lead metal in dark colour, while other features across the study are see in other colors. Also, pattern of the dark regions suggesting presence of lead in top soil clusters around the built-up areas. Therefore, attenuated lead concentration in soil detected are largely due to anthropogenic causes within the study area.

Figure 6 shows the distribution of lead metal across the study area based on the developed index by this study. The inclusion of a multiplicative constant of 10 was to exaggerate the raster output of the radio bands involved. It is therefore expected as seen in the legend of figure 8 that the least NDLI values should not be less than 10.

NDLI values across the study area ranges from 10-15; larger percentage of the region (equivalent to large percentage of distribution of vegetation across the study area), top soils in the far Northern and Southern region of the study area have least NDLI value (10-11), implying that lead pollution in these regions is the minimum in the entire study area. NDLI value ranges 12-13 (represented in yellow) in figure 8 corresponds to the detected lead distribution in top soil by the modified Kaufmann's relation. This range of values of NDLI (12-13) indicated in yellow represents region of top soil that cluster around the developed or built-up area in the study area. This is a validation of the tweaked Kaufmann's relations earlier presented and an indication that lead metal though occurs naturally on the Earth surface, its concentration and toxicity is increased by human activities.

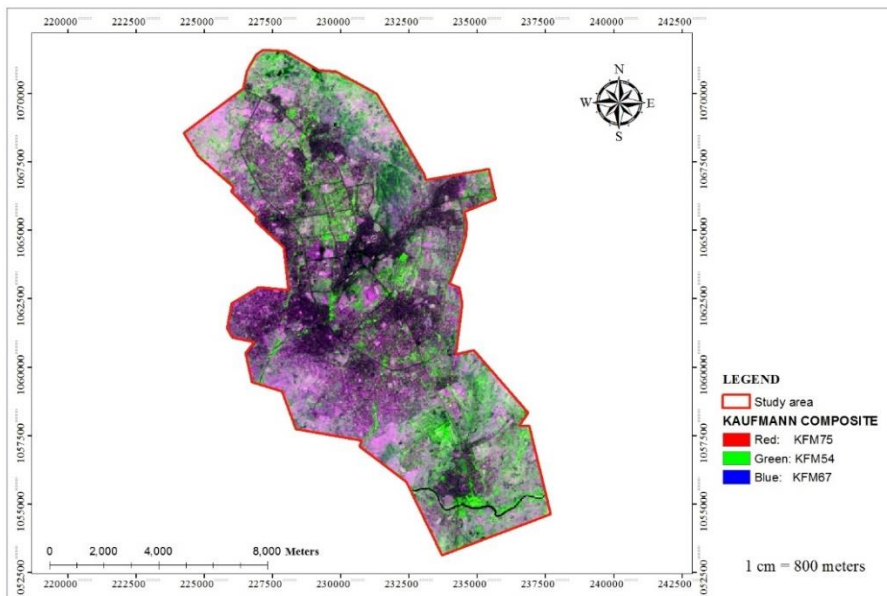


Figure 5: Colour composite from modified Kaufmann' relation obtained from Landsat 8 bands 7+5, 5+4, 6+7 in RGB sequence

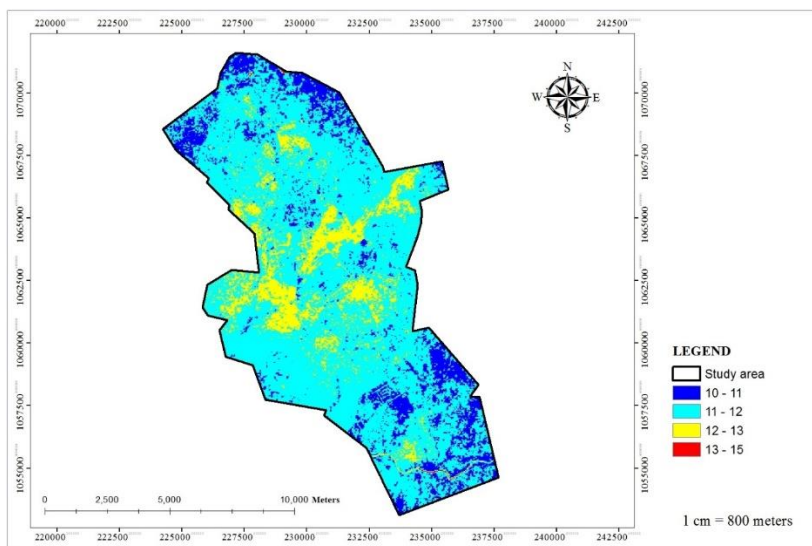


Figure 6: NDLI map of the study area.

Although not obviously visible, some raster cells in figure 6 and 7 have NDLI values ranging from 13-15, top soils in these raster cells have been regarded as the lead hotspots in the study area. In order to pin point top soils with high concentration of lead metal (where NDLI values ranges between 13 and 15), a map indicating these spots was produced in the ArcMap environment.

Figure 7 shows the distribution of top soils with highest NDLI values – 13-15 (lead hotspots). These hotspots are largely (6 out of 7) noticed around the central region of the study area where built-up land use is most significant. These points were thereafter visited and soil samples taken for AAS tests as a means of validating the study outcomes.

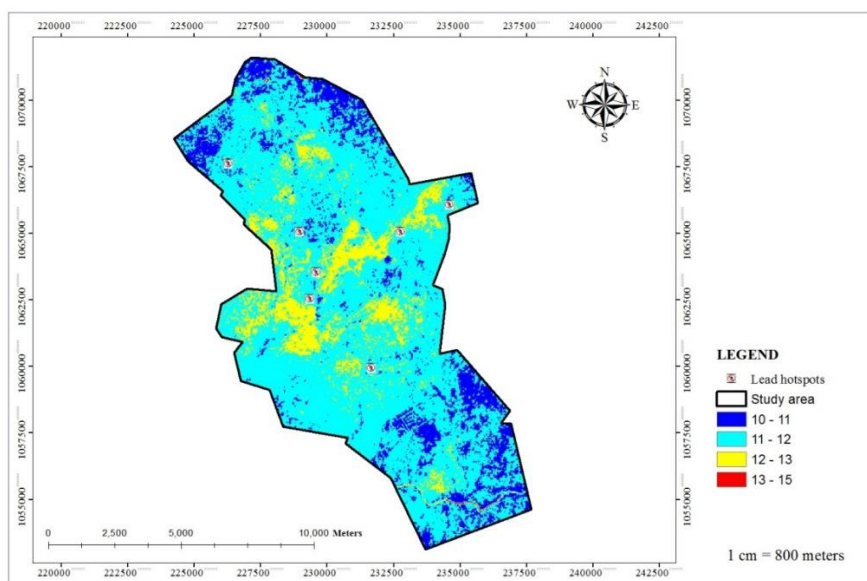


Figure 7: Overlay of lead hotspots on NDLI map of study area (hotspots shown in red)

Principal Component Analysis

Table 4 shows the Eigenvalues of the variance-covariance matrix output by the PCA of bands 3, 4, 5 and 6

The aim of PCA is to reduce the dimensionality of the input rasters to obtain only the most useful (one that carries the largest amount of information needed) principal components. Table 5 shows the eigenvalues of the four components (the extracted linear combination of the NDLI bands) from the PC analysis performed. Component 1 (PC1) however carries the largest amount of information (about 89%) followed by the second component (PC2) which carries about 7% of the information in the four bands (ratioed or combined). Therefore, the last two components (PC3 and PC4) could be discarded as they both merely carry 4% of information from the image channels.

This output in table 4 further implies by table 5 which shows that PC1 and PC2 are the significant bands needed from the input layers or bands. Hence, these two components have the least amount of correlation. Consequently, PC3 and PC4 are

discarded since they have higher correlation values with themselves (see table 5).

Columns of focus for analysis from table 6 are basically that of PC1 and PC2 since PC3 and PC4 are to be discarded.

In the PC2, there is a contrast observable in the signs and values of the PC's coefficients. The coefficient of the original 2nd band (band 5) had a high negative value (-0.7268) while the remaining bands had positive values (0.04325-0.54736). A plot of the PC1 and PC2 coefficients are presented in figures 8 (a – b).

In order to explore PC1 and PC2, the Eigenvectors of the variance-covariance matrix was analyzed as presented in table 6. Table 6 shows the Eigenvectors of the variance-covariance matrix.

The output raster for PC2 as shown in figure 8(b) has a direct relationship with 2nd band shown in table 6 (with negative value). It is deducible that the negative value is an indication of water bodies in PC2 (since the water body in the southern region of the study area is well highlighted on this PC). This therefore implies that PC2 is not carrying obvious information to detect the presence of lead.

Table 4: Eigenvalues of the variance-covariance matrix

Component	Eigenvalues	Percentage	Accumulative of eigene values
1	22427.25904	89.4461	89.4461
2	1679.257007	6.6973	96.1434
3	939.9883526	3.7489	99.8923
4	26.9953722	0.1077	100.000

Table 5: Correlation matrix

	PC1	PC2	PC3	PC4
PC1	1.00000	0.64669	0.78306	0.97827
PC2	0.64669	1.00000	0.84483	0.71216
PC3	0.78306	0.84483	1.00000	0.86340
PC4	0.97827	0.71216	0.86340	1.00000

Table 6: Eigenvectors of the variance-covariance matrix

	PC1	PC2	PC3	PC4
1st Band	0.22050	0.41810	0.40434	0.78299
2nd Band	0.45391	-0.72368	0.51977	-0.00981
3rd Band	0.78000	0.04325	-0.61949	0.07715
4th Band	0.37005	0.54736	0.42729	-0.61715

PC1 from table 5, carries the largest amount of information in the composite band (about 89%). The third band (band 6) in table 6 also has the highest value (0.78000) other than the other bands with values ranging from 0.2205-0.45391. This interprets that there is high likeliness that band 6 of landsat 8 (SWIR) can be used for mapping the presence of lead in soil. For the purpose of visualizing this effect, this component has been mapped to investigate its tendency of depicting the presence of lead across the study area (figure 8(a)).

PC1 has very dark region as well as the slightly dark, then grey region. The very dark obviously are water bodies in the study area and can be seen as a linear feature in the southern region. The slightly dark areas however show the same pattern as the lead polluted areas on NDLI map shown in figure 6 and 7. This therefore means that PC1 is enough to map out the presence of lead in soil in our area of interest.

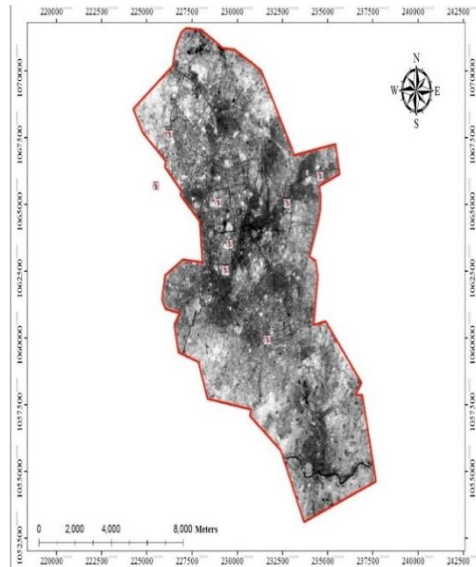


Figure 8(a): Principal component 1

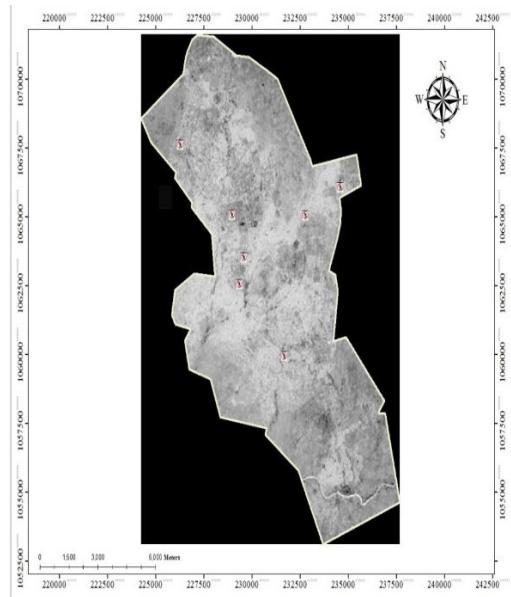


Figure 8(b): Principal component 2

Comparative analysis of the three approaches

Figure 9 shows relatable outputs of the three geospatial techniques employed in this study for the spectral analysis of lead metal in topsoil. Using the NDLI map (in the middle) as reference, the yellow-colored regions indicating presence of lead also exists in the other two maps (indicated in black). This implies that the three methods are consistent with themselves, and are useful for mapping lead tailings in top soils

Table 7 presents the results obtained from AAS tests carried out on the seven identified hotspot regions and 2 other areas not identified as hotspot (used as control). As seen, the seven identified hotspots (sample ID 1 – 7) had concentrated values higher than the expected standard range of lead allowable in top soils, while the remaining 2 samples (sample ID 8 and 9) used as controls had values within the normal range.

Also, it was observed that Sample ID’s 4, 5 and 7 had very large lead concentrates. This large lead concentrate in the three samples also correspond to the three points with NDLI of 14 and 15 in the NDLI map. This authenticates the lead index generated and confirms that for any given region, the higher the lead concentrate, the higher the NDLI value.

Furthermore, according to the World Health Organization (WHO) standard permissible and ideal value for Lead in Top soils as 0.1mg/L and 0.005mg/L (10ppm and 0.5ppm) respectively, the computed value of Heavy Metal Pollution Index (HPI) as computed by equation (3) is given in Table 8.

As seen in Table 8, all soil samples except samples 8 and 9 are heavily contaminated with Lead. This result is further consistent with the developed NLDI and validates the NDLI developed in this study.

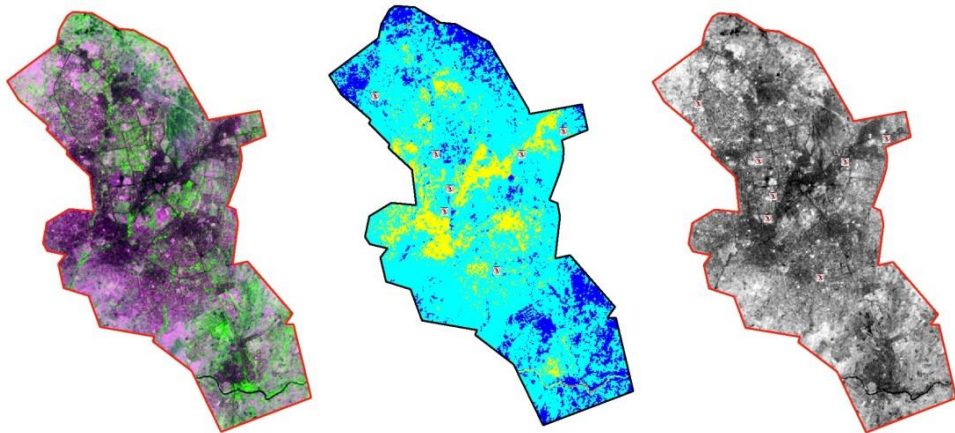


Figure 9: Comparison of the three methods

Table 7: Summary of AAS test result for 9 sample points

Sample ID	Analyte	Concentration (ppm)	standard value	Remarks
1	Pb	207.11	1 - 30	High
2	Pb	227.56	1 - 30	High
3	Pb	346.51	1 - 30	High
4	Pb	457.68	1 - 30	High
5	Pb	611.42	1 - 30	High
6	Pb	117.85	1 - 30	High
7	Pb	876.18	1 - 30	Very High
8	Pb	4.658	1 - 30	Normal
9	Pb	1.995	1 - 30	Normal

Table 8: HPI values for each sample

Sample ID	Concentration (ppm)	HPI value	Remarks
1	207.11	217.48	Contaminated
2	227.56	239.01	Contaminated
3	346.51	364.17	Contaminated
4	457.68	481.24	Contaminated
5	611.42	643.07	Contaminated
6	117.85	123.53	Contaminated
7	876.18	921.77	Contaminated
8	4.658	4.38	Not contaminated
9	1.995	1.57	Not contaminated

Conclusion

Three remote sensing (geospatial) techniques for investigating the spectral characteristics of lead tailings in top soils have been presented in this study using Minna metropolis as the study area. Using different Landsat 8 bands ratios and combinations, the study discovered a modified Kaufmann's relations, self-developed NDLI and PCA-based approach that are capable of characterizing the lead concentration level in the regions within the study area where topsoil is polluted by lead metals. Having established that lead metals exist across top soil in the study area at different concentrations, it is observed that the resultant results from the techniques had a near-zero standard deviation; which serves as validation of the effectiveness of geospatial techniques at mapping lead metals in top soil. Furthermore, the results obtained from the geospatial analysis via remote sensing were consistent with AAS test results and the computed HPI values; thus, validating the reliability of the presented methods for detecting and mapping lead contamination in top soils.

Acknowledgement

The authors sincerely appreciate TETFUND and the Federal University of Technology, Minna for the research grant with grant No. TETFUND/FUTMINNA/2019/B7/09 from which this study was funded.

References

- Aransiola, A. B and Odumosu, J. O. (2021). Prospectivity mapping for Gold Mineralization using Landsat 8 OLI image in Niger state. School of Environmental Technology International Conference (SETIC) 2020. Sustainable housing and land management, Federal University of Technology, Minna, 3rd – 5th May, 2021.
- Azibuike C. C, Chikere C. B and Okpokwasili G.C. (2016). Bioremediation techniques – classification based on site of application: principles, advantages, limitations and prospects. *World Journal of Microbiology and Biotechnology* 32, 180. <https://doi.org/10.1007/s11274-016-2137-x>
- Dhirendra Kumar and Ekhlague Khan (2021). Remediation and detection techniques for heavy metals in the environment. In book: *Heavy Metals in the Environment* (pp. 205-222), DOI:[10.1016/B978-0-12-821656-9.00012-2](https://doi.org/10.1016/B978-0-12-821656-9.00012-2)
- Grobelak A. and Napora A. (2015). The Chemophyto stabilisation Process of Heavy Metal Polluted Soil. *PLoS ONE*, 10 (6), e0129538. <https://doi.org/10.1371/journal.pone.0129538>.
- Ibrahim S, Kaduk J, Tansey T, Balzter H. and Umar Mohammed Lawal (2021) Detecting phenological changes in plant functional types over West African savannah dominated landscape, *International Journal of*

- Remote Sensing, 42:2, 567-594, DOI: 10.1080/01431161.2020.1811914.
- Jackson Wheeler (2021). Lead. An online resources available on: <https://www.belmontmetals.com/product-category/lead/>, accessed on 11 Nov., 2021.
- Jacquelyn Cafasso (2018). Lead Poisoning: Causes, Symptoms and Diagnosis. Available online: <https://www.healthline.com/health/lead-poisoning>. [Accessed on: 20th December, 2021].
- Jin, J., Zhou, X. P. and Ma, K (2018). The analysis of the optimum band combination based on the image of Landsat 8—A case study of thematic survey of heavy metals in soils in the mining area of Bayan Obo. *J. Inner Mongolia Univ.. Sci. Technol.* 35(1), 37–41
- Liu, M., Wang, T, Skidmore, A. K and Liu, X. (2018). Heavy metal-induced stress in rice crops detected using multi-temporal Sentinel-2 satellite images. *Sci. Total Environ.*, 18 (29), 637–638.
- Kolawole, T.O., Olatunji, A.S., Jimoh, M.T., Fajemila, O.T. (2018). Heavy metal contamination and ecological risk assessment in soils and sediments of an industrial area in Southwestern Nigeria. *Journal of Health Pollution* 8 (19), 180906
- Krishnendu Banerjee, Surajit Panda, Ayyemperuman T. J and Manish Jain (2019). Landsat 8 OLI Data for identification of hydrothermal alteration zone in Singhbhum Shear zone using successive band depth difference technique – A new image processing approach. *Journal of Current Science*, vol. 116, No. 10, pp. 1639-1647
- Latif Ab W., Anjum Ara and Jawed A. U (2013). Lead toxicity: a review. *Journal of Interdisciplinary Toxicology*, 8(2): 55–64.
- Mia, M. B. and Fujimitsu, Y. (2012). Mapping hydrothermal altered mineral deposits using Landsat 7 ETM+ image in and around Kuju volcano, Kyushu, Japan. *Journal of Earth Systems Science*, 121 (4), 1049 – 1057.
- Minna Master Plan, 1979
- Muszynska, E. and Hanus-Fajerska, E., 2015. Why are heavy metal hyperaccumulating plants so amazing? *Biotechnologia*. 96 (4). Available from: <https://doi.org/10.5114/bta.2015.5773>
- Q.Nabulo et al, 2012
- Nigerian National Population Census 2006
- Ilugbo, A.O, Adebo, A. B., Ajayi, O. A and Adewumi, O. O and Edunjobi, H. O (2018). Geophysical and geotechnical studies of a proposed structure at Akure, Southwestern Nigeria. *Journal of Engineering Research and Reports*, 2 (2), DOI: 10.9734/JERR/2018/42181.
- Peng, Y., Kheir, R. , Adhikari, K, Malinowi, R, Greve, M, Knadel, M and Greve, M. (2016). Digital mapping of toxic metals in Qatari soils using remote sensing and ancillary data. *Journal of Remote Sensing* volume 8, 1003, pp. 1-19.
- Qu Y. H *et al.* (2015). Mapping analysis of heavy metal elements in polluted soils using laser-induced breakdown spectroscopy. *Journal of Spectroscopic Spectral Analysis*, vol. 3, pp. 982-989
- Sadiya, T. B. and Ozigis, M. (2015). Mineral Detection and Mapping Using Band Ratioing and Crosta Technique in Bwari Area Council, Abuja Nigeria. 5.
- Seema Timari, Indra Prasad T. and HI Tiwari (2013). Effects of Lead on Environment. *International Journal of Emerging Research in Management and Technology*, volume 2, issue – 6, pp. 1-5.
- Souza IC, Duarte ID, Pimentel NQ, Rocha LD, Morozesk M, Bonomo MM, Azevedo VC, Pereira CDS, Monferrán MV, Milanez CRD, Matsumoto ST, Wunderlin DA, Fernandes MN (2013) Matching metal pollution with bioavailability, bioaccumulation and biomarkers response in fish (*Centropomus parallelus*) resident in neotropical

- estuaries. *Journal of Environmental Pollution* 180:136–144.
- Wang F. H and Gao J (2018). Hyperspectral sensing of heavy metals in soil and vegetation: feasibility and challenges. *ISPRS Journal of Photogrammetry and Remote Sensing*, 136, pp. 73-84.
- Xie L., Hao P., Cheng Y., Ahmed I. M., Cao F. (2018). Effect of combined application of lead, cadmium, chromium and copper on grain, leaf and stem heavy metal contents at different growth stages in rice. *Journal of Ecotoxicology of Environmental Safety* 162, pp. 71–76. [10.1016/j.ecoenv.2018.06.072](https://doi.org/10.1016/j.ecoenv.2018.06.072).
- Yang Q., Li Z., Ma H., Wang L. and Martin J. D. (2016). Identification of the hydrogeochemical processes and assessment of ground water quality using classic integrate geochemical methods in the Southeastern part of Ordos basin, China. *Journal of Environmental Pollution*, doi.: <https://doi.org/10.1016/j.envpol.2016.08.017>.
- Yang Yang, Andrew C. Chang, Meie Wang, Weiping Chen and Chi Peng (2018). Assessing cadmium exposure risks of vegetables with plant uptake factor and soil property. *Journal of Environmental Pollution*, volume 238, pp. 263-269.
- Yin, P., Shi, L., (2014). Remediation of Cd, Pb, and Cu-contaminated agricultural soil using three modified industrial by-products. *Journal of Water Air and Soil Pollution*, 225 (11), 2194.
- Yun Yang, Qinfang Cui, Peng Jia, Jinbao Liu and Han Bai (2021). Estimating the heavy metal concentrations in topsoil in the Daxigou mining area, China, using multispectral satellite imagery. *Sci Rep* **11**, 11718 (2021). <https://doi.org/10.1038/s41598-021-91103-8>.
- Zhao Ji, Yanfei Zhong, Xin Hu, Lifei Wei, Liangpei Zhang (2019). A robust spectral-spatial approach to identifying heterogenous crops using remote sensing imagery with high spectral land spatial resolutions. *Remote Sensing of Environment*, volume 239, <https://doi.org/10.1016/j.rse.2019.111605>.